Journal of Electron Microscopy **49(4)**: 517–524 (2000)

Full-length paper

Zero loss peak deconvolution for bandgap EEL spectra

B. Rafferty[1,2,*], S. J. Pennycook[1] and L. M. Brown[2]

[1]Solid State Division, Oak Ridge National Laboratory, Oak Ridge, TN 37831-6030, USA, and [2]Cavendish Laboratory, Madingley Road, Cambridge CB3 0HE, UK

*To whom correspondence should be addressed. E-mail: dr.rafferty@physics.org

Abstract This paper shows how bandgap EEL spectra are commonly processed either by deconvolution or subtraction methods in an attempt to remove effects arising from the finite width and long tail of the zero loss peak. This paper will compare the two main methods, and show that the deconvolution method is significantly more reliable and free of user-interpretation or artefacts. We first consider how the zero loss peak is produced and what effects experimental conditions have upon it, and then show that only by the deconvolution method can accurate bandgap energies and bandgap densities of states be determined.

Keywords scanning transmission electron microscopy, electron energy loss spectroscopy, deconvolution, optoelectronic

Received 8 February 2000, accepted 15 April 2000

Introduction

The ability to view the bandgap region of semiconducting and insulating materials is an ideal way to study their electronic structure. Optical techniques for studying the bandgap region have the advantage of high-energy resolutions of ~1 meV which allow fine detail to be resolved within the spectra. However, the light sources used will limit the spatial resolution to ~1 micron, so that only measurements of the macroscopic properties can be studied. The EELS technique used here has the considerable advantage of high spatial resolution. Here we use a VG HB501 scanning transmission electron microscope (STEM) where the electron beam can be focussed to ~5 Å and positioned anywhere on the sample. The energy resolution of the EELS system (0.22 eV) is much worse than the optical case, but it is possible to extract data with an accuracy of ~50 meV, which is noise-limited, and determine the nature of the bandgap from the resulting spectra [1].

The energy resolution of an EELS system is defined by the zero loss (ZL) peak; however, it is sometimes not appreciated that it is the extended tails of this peak and not the main peak width itself that are the source of the problems in producing good bandgap spectra. The ZL peak in the EEL spectra typically has a full-width at half-maximum (FWHM) of 0.27 eV, which is asymmetric and has a large region that tails into the EEL spectrum by as much as 15 eV. The intensity of the ZL peak is ~10^4 times the intensity of that produced by the bandgap excitation processes. Moreover, the intensity of the tails of the ZL peak is at least equal to the bandgap signal. Other than the problems with the nature of the ZL peak, there are also practical problems that must be overcome. To correct for any energy drift between consecutive acquisitions (due to the stability of the beam-blanking reference voltages), the ZL peak must hit the CCD camera and also be undersaturated because the ZL peak is used as an energy reference marker. For each individual spectrum acquired in this way, the bandgap signal will only be a few counts, and so many spectra must be acquired to produce a spectrum with a good signal/noise ratio. This normally requires the acquisition of 500–1000 spectra, the smaller the bandgap the higher the number of spectra required. To take full advantage of the energy resolution of the spectrometer, a high dispersion must also be used (0.05 eV channel^{-1}) when acquiring the spectra. A poorly sampled measure of the ZL peak will result in a degradation of the measured energy resolution.

Once we have summed all the individual spectra, the ZL peak must then be removed to reveal the bandgap onset or any other low-energy features of interest. There are two main ways in which this can be achieved, which we compare as regards accuracy and reliability. The first

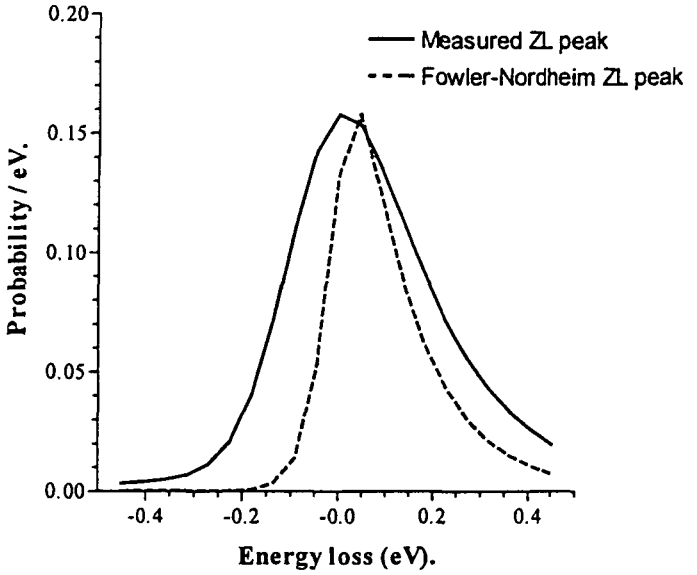

Fig. 1 Plot comparing a measured ZL peak with that predicted by Fowler–Nordheim theory. The tails of the calculated curve do not match those of the measured curve.

and most commonly used method involves a scaled subtraction of a measured or modelled ZL peak from the EEL spectrum of the sample. Attempts to model the ZL peak [2] have had some success at fitting the main intensity of the peak, but have large discrepancies in the tails of the order of 25–35% depending on the noise level. The second method involves a deconvolution of the ZL peak from the EEL spectrum to remove its tails. Deconvolution methods have been widely used to remove multiple scattering contributions in EEL spectra [3] and also to enhance the energy resolution of spectra by making use of the asymmetry of the ZL peak [4]. In this paper we first consider how the zero loss peak is produced and what effects experimental conditions have upon it, and then show that only by the deconvolution method can accurate bandgap energies and bandgap densities of states be determined.

The zero loss peak

When the electrons strike the sample, most of them are elastically scattered and transfer no energy to the sample. These electrons make up the zero energy loss peak and form the most intense feature in the whole of the EEL spectrum. Ideally the ZL peak would have no width, the electron beam would be perfectly monochromatic; correspondingly, it would appear as a delta function in an EEL spectrum. In practice this is not so and the ZL peak not only has a finite width but is also asymmetric. To be able to remove the ZL peak in a satisfactory manner it is useful to know what factors affect the shape of it. This will also help in understanding how a STEM/EELS system should be aligned. At the same time, this will minimize the width of the ZL peak allowing the highest energy resolution spectra to be obtained without the loss of any fine structure in the EEL spectra.

There are many factors that affect the shape of the ZL peak to some degree. The trick to the problem lies in knowing which are important and so have the largest contribution to the structure of the ZL peak. Starting from the base of the column of the STEM and following an electron to the CCD camera we shall see where the electron's energy distribution can be changed.

The first point to consider is the field-emitting tip. The electrons tunnel out of the tip at a rate that depends on the energy level of the electron relative to the Fermi level of the tip. The emitted electrons will now have a range of energies. Once the electrons have left the tip they are accelerated to an energy of 100 keV. Electronic instabilities in the high-voltage tank will cause the position of the electron energy distribution to wobble around and give the appearance of a broader total energy distribution (TED) for the electrons. In practice these instabilities are on much longer time scales (1–10 s) than the typical exposure time of a low-loss spectrum (~20 ms) and have no real influence on the acquisition of bandgap spectra; thus proposed energy stabilizer systems will not improve the quality of present bandgap spectra. Chromatic aberration of the objective lens will not visibly affect the TED and so can be ignored.

The spectrometer is the next source that contributes to the width of the TED. The Issacson's sector magnetic prism that is attached to the STEM has been optimized (in the design adopted by VG microscopes), so that a monochromatic beam of electrons can be focused to a point on its vertical plane of symmetry. There are aberrations associated with the spectrometer, the extent of which depend on the height of the specimen in the objective lens (causing second order aberrations), and the position and angle at which the beam enters the spectrometer. The curvature of the entrance and exit faces along with several multipoles at the entrance to the spectrometer allow for the correction and reduction of second, third and even fourth order aberrations [5]. For large collection angles the entrance multipole coils contribute significant aberrations that can dominate the spectrometer aberrations and so put an upper limit on the size of collector apertures that can be used for high-energy resolution work. Poor alignment of the spectrometer and its multipoles can increase the width of the TED by 20 eV or more. However, if correctly aligned the contribution can be lowered to as low as 20 meV.

Once the electrons leave the spectrometer, the dispersed image of electrons is then focused onto a scintillator by three quadrupoles. If the electron beam has to pass through these quadrupoles at large angles then they could introduce more aberrations due to the non-uniform fields at high angles. The effect can be eliminated by mechanically and electrically aligning the quadrupoles onto the

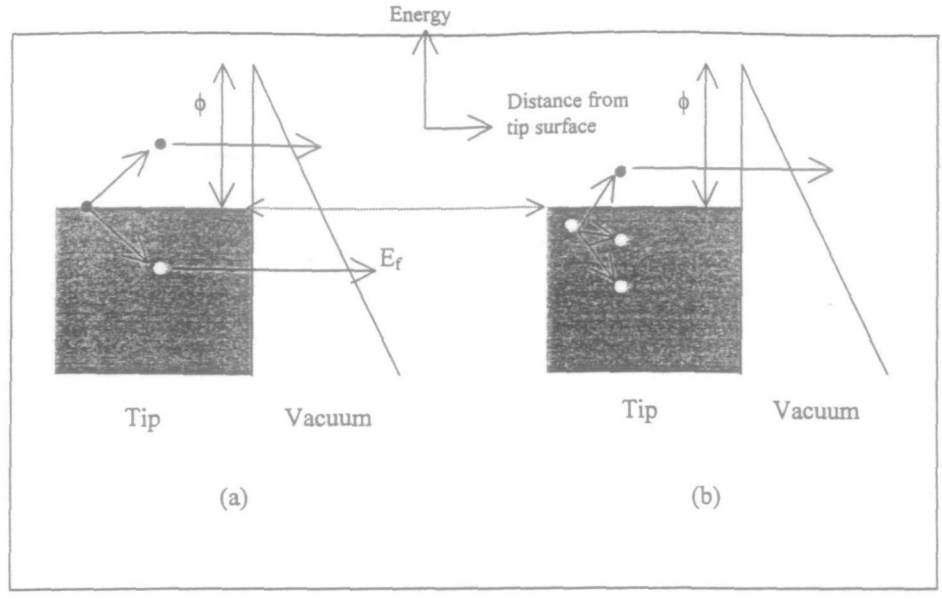

Fig. 2 (a) A schematic diagram showing the simultaneous two-particle tunnelling producing a symmetric contribution to the zero loss peak. (b) A schematic diagram of the hot hole decay process.

optic axis of the microscope. The electrons hitting the scintillator produce photons that are then optically focused onto the CCD camera. Some of the photons produced can be transversely scattered in the scintillator. This enlarged illumination is then mirrored on the CCD and seen as a degradation of the energy resolution. This effect only becomes significant if the beam current is very high; otherwise this additional signal is below the noise level in the bandgap spectra. Also if too many photons hit any particular pixel on the CCD then that pixel becomes saturated and the electrons leak into neighbouring pixels, again resulting in an increased width of the TED. Low exposures can be used to avoid these forms of energy spread in the EEL spectra.

The spectrometer alignment is the most critical optical factor in reducing the spread of the ZL peak, if correctly aligned the optics can add as little as 30–50 meV to its width for collection angles less than 10 mrad [6]. This is much lower than typical widths of ZL peaks (0.3–0.7 eV). We shall now discuss how the field emission tip itself can affect the ZL peak.

Historically, Fowler and Nordheim [7] first derived an expression for the total current field-emitted from cold metals. This derivation was based upon a free-electron model for the electrons in the tip. An applied external field pulls the vacuum level outside the tip to below the Fermi level of the electron gas allowing the distributed electrons across the Fermi level to tunnel out of the tip. The resulting tunnelling current, $j(E)$, is proportional to the product of the Fermi distribution and the tunnelling probability,

$$j(E) \propto \frac{\exp(E/d)}{1 + \exp(E/k_B T)}, \qquad (1)$$

$$d = 0.976 \frac{F}{\sqrt{\phi}}$$

where F is the applied electric field (V Å^{-1}), ϕ is the work function (eV) and E is the energy (eV) of the electron above the Fermi level (the negative of the energy loss as measured in the EEL spectrum). The intensity of the main portion of the ZL peak fits relatively well to that predicted by Fowler–Nordheim theory, but fails for the intensity on the tails of the ZL peak as shown in Fig. 1. The extra tunnelling current can be accounted for when exotic scattering events in the tip are considered. A full review of the field emission of electrons from tips and their TEDs has been presented elsewhere by Gadzuk and Plummer [8]. A few of the scattering processes will be outlined here that are based upon their work.

Virtual scattering events can take place in the metal near the Fermi surface whose result is to scatter an electron to an energy δ above the Fermi level and another below by an equal amount of energy as shown in Fig. 2a. Because all the states below the Fermi level are filled at low temperatures, this process remains virtual in the absence of an applied external field. If the electron scattered to the low-energy state can tunnel out of the tip then the process becomes real. The higher energy electron will have an enhanced tunnelling probability and the two electrons will contribute to extra current in the tails of the ZL peak. This simultaneous two-particle tunnelling

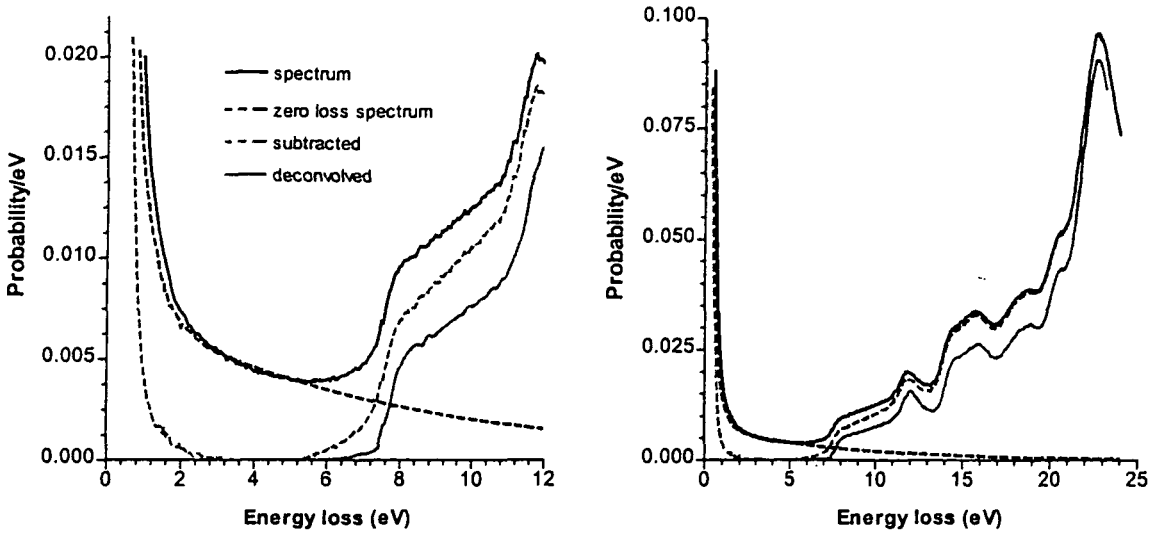

Fig. 3 A comparison of the subtraction and deconvolution methods. The deconvolution routine shows a clear bandgap onset with no detectable bandgaps states.

process, however, will contribute equal numbers of electrons to either side of the ZL peak, producing a symmetric broadening, but the observed intensity of the tails is asymmetric.

Another process is based upon the electron cascade of a hot hole. Suppose an electron below the Fermi level has tunnelled out of the tip, it leaves behind a hot hole. This hot hole can then be scattered by the electron gas producing a secondary hole and electron as shown in Fig. 2b. The interaction occurs via a momentum- and frequency-dependent screened Coulomb interaction that involves the dielectric properties of the electron gas. This scattering event is analogous to the scattering of fast electrons by a thin film. The scattering probability depends on the imaginary part of the reciprocal dielectric function. The electron produced by the hole decay may then tunnel out of the tip and be observed in the tail of the ZL peak. The process causes extra current from the electrons initially well below the Fermi level, in agreement with the observed asymmetry. There are many other scattering events that can be envisaged, e.g. emission from narrow d-bands at the surface of the tip and resonant tunnelling models. The TED of the electrons emitted from a field-emitting tip is therefore very complicated. Although in principle it should be possible to model the ZL peak, in practice this will be unreliable as many of the extra scattering processes depend critically on the surface cleanliness and geometry of the tip. Each time the tip is cleaned ('flashed'), a new ZL peak would have to be calculated with a set of best-guess parameters defining the new state of the tip. Therefore, it would be better to just measure the EEL spectrum with the electron beam passing though a hole in the sample. This method would be much more satisfactory to use as it is a true measure of any and all effects that can change the shape of the ZL peak.

If the STEM and PEELS system is aligned accurately then ~80% of the width of the ZL peak comes from the energy distribution of the emitted electrons from the tip. For a relatively sharp tip (radius of curvature ~40 nm) the width of the ZL peak can be brought down to a FWHM of 0.27 eV. It will be seen later that this corresponds to an energy resolution in EEL spectra of ~0.22 eV.

Removal of the zero loss peak

Once we have acquired our bandgap EEL spectra we have to decide which method will be employed in the removal of the ZL peak; subtraction or deconvolution? We shall compare both methods starting first with the subtraction.

Scaled subtraction of the zero loss peak

When carrying out a scaled subtraction of the ZL peak we need first to ask two questions: what shall we use as the ZL peak, and to which part of the bandgap EEL spectrum do we scale the ZL spectrum? We have already seen that to try and model the ZL peak would entail substantial uncertainty in the modelled peak. Only a measured experimental ZL peak will suffice. To answer the second question we must now select an energy window over which the integrated intensity of both the ZL and bandgap EEL spectra must be matched.

The choice of the normalization energy window reveals the fundamental flaw of the subtraction method. The measured ZL peak does not match the shape of the ZL peak in the spectrum from the sample. If the user scales the spectra with an energy window from $-\delta$ to $+\delta$ centred on the ZL peak, then a relatively good fit with small errors can be made to the main peak intensity. However, because of the difference in shapes of the peaks the fit in the tail region can result in very large errors

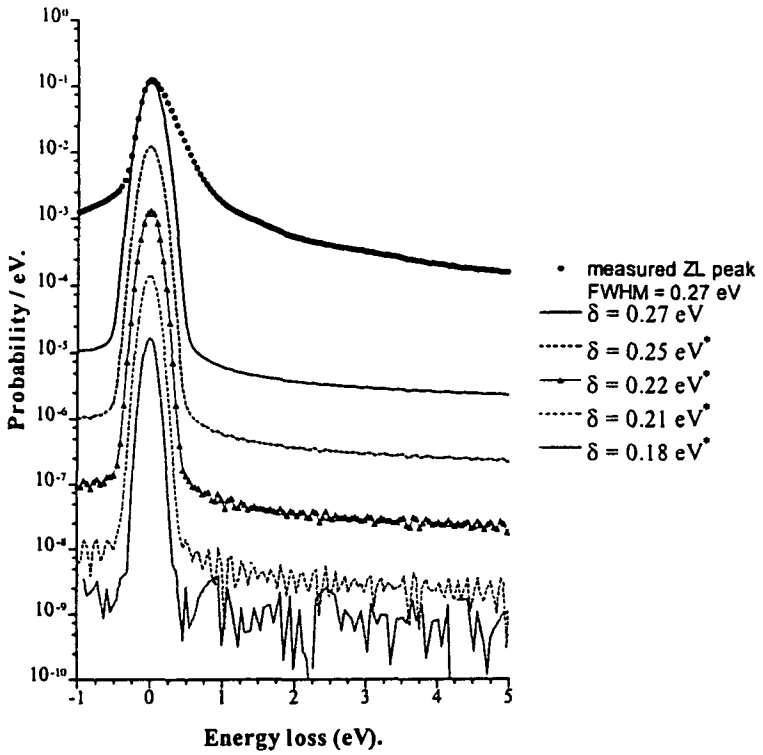

Fig. 4 A comparison of the effects of different widths of the modified resolution function on the deconvolution routine. Trying to deconvolve below the true energy resolution generates excessive noise obscuring the spectral detail. It can also be seen that the routine considerably reduces the intensity in the tails of the zero loss peak by two orders of magnitude. δ is the FWHM of the modified resolution function. The deconvolved spectra marked with an asterisk have been reduced in magnitude by successive factors of 10 from that of the 0.27 eV deconvolved spectrum for display purposes.

revealing 'bandgaps' of arbitrary sizes. An energy window in the range + δ to + Δ ($\Delta < E_g$) is commonly used in scaled subtractions and the errors in the scaling at 0 eV ignored. This method can reveal bandgap values that seem more reliable. Figure 3 shows such a scaled ZL peak subtraction for spectra taken from bulk MgO. The subtraction has produced a spectrum that reveals a bandgap that agrees quite well with the accepted optical measurement. This method has left relatively large tails at the onset to the bandgap and so has not been able to reveal the shape of the bandgap onset. The same spectrum processed using the deconvolution routine, presented in the next section, is also displayed. The intensity preceding the bandgap onset in the subtracted spectrum has been all but removed. If we had a material with a smaller bandgap we would be forced to use a smaller energy window for the fitting or use more of the main part of the ZL peak and run into the errors previously mentioned. So far we have assumed the intensity within the bandgap to be zero, but this may not be the case especially if the spectrum was from a region that contained a grain boundary, defect or surface (as will be seen later). Indeed determination of such effects is one of the most important applications of EELS to optoelectronic materials. The presence of any structure in the bandgap completely negates the premise upon which a scaled subtraction is based, and renders it useless for such studies.

Deconvolution of the zero loss peak

The ZL peak shows the response of the STEM and PEELS system to electrons that have suffered no energy loss. This will also be the response for electrons that have undergone any particular transition. Thus, each channel x in the EEL spectrum will have this response imposed upon it. The 'ideal' spectrum, $i(x)$, has been convolved with the zero loss spectrum, $z(x)$. Thus, a deconvolution of the zero loss spectrum from the recorded EEL spectrum, $r(x)$, is the only way to remove the true effects of the ZL peak. We have,

$$r(x) = i(x) \otimes z(x) \tag{2}$$

Some care must be taken in the deconvolution routine because the data are discrete, finite in size and most importantly contain noise. In Fourier space the solution we seek is

$$I_k = \frac{R_k}{Z_k} \tag{3}$$

For high-frequency components the above Fourier ratio is dominated by noise, and large oscillatory artefacts dominate the final deconvolved spectrum. There are many ways in which to overcome this problem, e.g. the Wiener filter deconvolution. Rather than transforming R_k with the operator Z_k^{-1}, a small real positive quantity is added to the denominator. Hence, Z_k^{-1} is replaced with

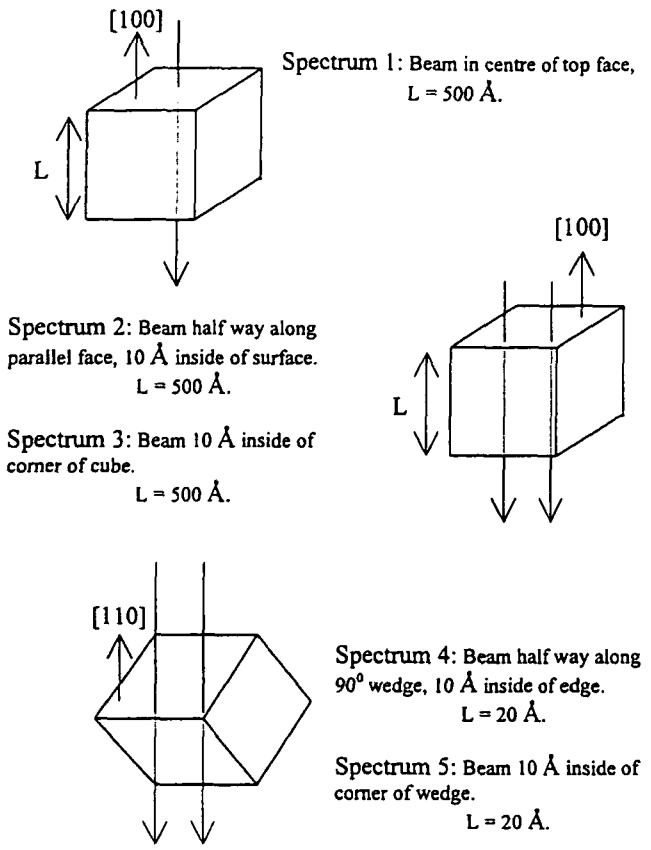

Fig. 5 A schematic diagram showing the different geometries of the MgO cubes and the electron beam positions that were used to acquire the spectra. L is the approximate path length of the beam through the cube.

$$\frac{Z_k}{|Z_k|^2 + |N_k|^2} \tag{4}$$

This method is robust but care must be taken with the choice of N_k and the computational setup of the routine. Another method that is conceptually easier to follow is the Fourier-ratio method [3]. This is the method used here as it is the least likely to be influenced by the user and it is clear to see when the routine has not been used correctly, as will be demonstrated. The final deconvolved data, $f(x)$, are assumed to be the convolution between the ideal data, $i(x)$, with some modified resolution function, $m(x)$, whose width is necessarily less than that of the ZL function, $z(x)$. The choice of $m(x)$ depends on your needs; for bandgap EEL spectra it is the tails of the ZL peak that are the problem and not the main peak intensity. A deconvolution routine that removes the main peak intensity and leaves the tails is quite useless for bandgap EEL spectra. For this reason a Gaussian peak is used as the modified resolution function. A Gaussian has relatively small tails, compared to, e.g. a Lorentzian peak, and is conveniently represented in both real and Fourier space. Thus,

$$f(x) = i(x) \otimes m(x)$$

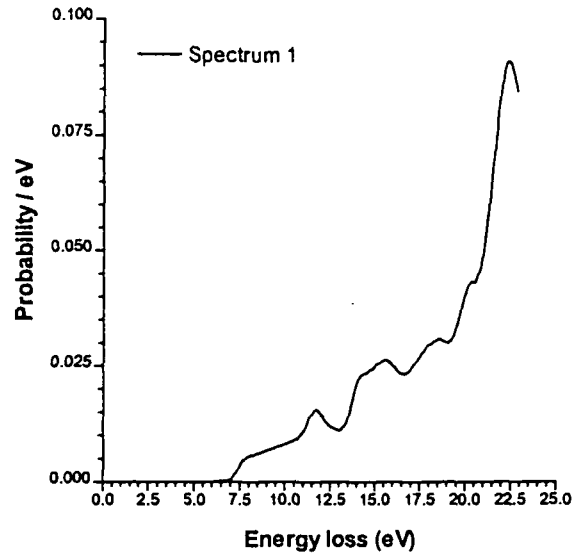

Fig. 6 Spectrum 1 showing the low-loss spectrum of the MgO cube, the bulk plasmon peak dominates the spectrum and no intensity within the bandgap is apparent.

$$F_k = M_k \frac{R_k}{Z_k} \tag{5}$$

The width of $m(x)$ is chosen so that its high-frequency components are sufficiently small that the noise components in R_k and Z_k are suppressed. The modified resolution function basically acts as a smoothing operator on the Fourier-ratio. There is a limit to how narrow the modified resolution function can be, which depends on the actual resolution and the noise level in the data. If it is too narrow then high-frequency artefacts dominate the fine structure of the resulting deconvolved spectrum. The smallest width of $m(x)$ that does not introduce unacceptable high-frequency artefacts is a better measure of the true energy resolution of the EEL spectrum. The difference in the FWHM of $m(x)$ and $z(x)$ is largely due to instabilities during the acquisition of the spectra. Figure 4 shows deconvolved spectra for a range of widths used for the modified resolution function that are above and below the true energy resolution limit. The original ZL peak, of FWHM = 0.27 eV, is also displayed to show how effectively its tails are removed. It can be seen that for a Gaussian of width less than 0.22 eV the high-frequency noise components start to dominate the spectral features and show clearly when the user has tried to extract too much information out of the data. In this case, the energy resolution has been improved by 50 meV, indicating that the instabilities during the acquisition of the spectra were as low as 50 meV.

The deconvolution method presented here has many advantages over a direct subtraction of the ZL peak. The deconvolution is technically the correct way to remove the ZL peak. The routine introduces fewer, if any at all, user artefacts, because it is independent of the size of the

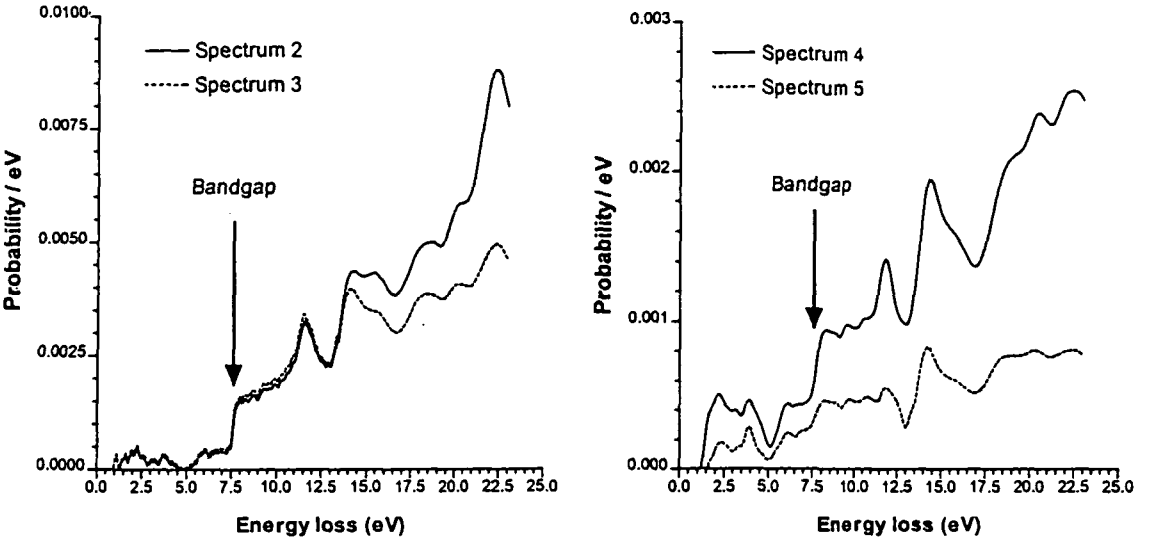

Fig. 7 (a) Bandgap spectra taken with the cube aligned along the [100] direction. There is a small amount of intensity within the bandgap which is above the nose level. (b) The equivalent spectra as in (a) with a cube now aligned along the [110] direction. The small intensity within the bandgap is now enhanced due to the reduction in the excitation volume. The defect structure can now clearly be seen.

bandgap. It preserves any real structure that may be present within the bandgap and can be used to reveal information down to an energy loss of ~ 0.9 eV. Any information below this energy that may be present cannot be extracted with today's field emission tips; data below this level can be disregarded. Deconvolution routines are renowned for increasing the noise level in data. However, this is only a problem when you intend to increase the resolution beyond the actual resolution with which the data have been acquired [4]. Noise is not enhanced when deconvolution is used only to remove probe tails, and the deconvolved spectrum only needs the resolution of the actual ZL peak.

In the next section we shall see that defect states within the bandgap of MgO can be extracted from the raw data even when their contribution is small compared to the bandgap signal itself.

MgO defect states

The regular cuboid shape of MgO smoke cubes allows them to be easily aligned using either direct imaging or microdiffraction techniques in STEM. The electron probe can then be positioned anywhere on the cube and an EEL spectrum taken from that point. The spectra presented here were acquired with a McMullan-type PEEL system on a VG HB501 STEM in reduced area scan mode at a magnification of ×10 million (equivalent to an area of ~20 × 20 Å). These conditions were chosen so that the electron beam could be re-positioned onto a particular feature, e.g. the edge or corner of a cube using the dark-field image, while a series of spectra were being acquired to correct for any possible specimen drift. Typically between 500 and 1000 individual spectra were acquired to make up one final spectrum. After a series of spectra had been acquired, a spectrum in the region of the carbon K-edge was acquired to check that there was no carbon contamination during acquisition. All of the spectra were deconvolved with the ZL peak and deconvolved to remove any contributions from multiple scattering. The resulting single scattering spectra were then normalized so that the intensity is in units of probability per electron volt.

Figure 5 shows a schematic diagram of the orientations and positions of the MgO cubes and the electron probe, respectively, for the different spectra that were acquired. Spectrum 1 in Fig. 6 has been taken from the centre of a cube with the beam parallel to the [100] pole. Spectra 2 and 3 in Fig. 7a were then taken from the middle of one of the faces and along the edge between two faces of the cube, respectively. For spectra 4 and 5 in Fig. 7b the equivalent spectra to 2 and 3 were acquired this time with the cube tilted so the beam was parallel to the [110] pole.

Spectrum 1 is dominated by the excitation of the bulk plasmon peak. There is no discernible intensity within the bandgap that could be associated with any defect states. However, defects in MgO are easily generated by knock-on effects produced by the electron beam. Displacement energies are reduced at sample surfaces, thus we expect these defects to be concentrated at the surfaces of the sample. For the bulk spectrum the surface contributions are only a small fraction of the illuminated volume. On positioning the electron beam along the surfaces or edges of the cube we physically reduce the excitation volume and thus the bulk contributions. The precise way in which the bulk, surface and corner excitation modes are affected is detailed elsewhere [9–13]. Suffice it to say that with the beam closer to a surface the relative

contribution is greater. In spectra 2 and 3 there is now residual intensity within the bandgap, which is just above the noise level in the data. There seem to be three contributing peaks in the bandgap at energies of ~2, 4 and 6 eV. The structure of this intensity is the same in both spectra, which would be quite a coincidence if it were either noise or an artefact of the deconvolution routine. Tilting the cube over to the [110] pole and acquiring the equivalent spectra further reduces the bulk contributions, and the intensity above the bandgap onset is dominated by surface and corner excitation modes. The intensity within the bandgap is now greatly enhanced and the detail of the defect states is revealed in full. There are peaks at 2.3, 3.4, 4 and 6.2 eV. The enhancement of the defect states with decreasing the size of the excitation volume would imply that the defect states within the bandgap are in fact surface defects. Walls [14], Henrich [15] and Kassim *et al.* [16] have presented work on the surface defect states of MgO cubes previously. Walls showed the peak at 3.4 eV to be induced by the electron beam, for low currents this peak can be eliminated altogether. The peaks at 2.3 and 6.2 eV are associated with the {100} surfaces of the cubes [15], in particular, these losses could be produced by surface F-centres formed when oxygen atoms are knocked out of the crystal structure [16].

Conclusions

It has been demonstrated in this paper that the extended tails present on the ZL peak can be removed using a deconvolution routine that will reveal defect states down to energy losses of 1 eV without compromising the integrity of the original data. The only way to lower this limit without enhancing the noise level will be by the use of monochromators, e.g. that proposed by Batson [17]. A comparison of the deconvolution routine and a scaled subtraction has shown that the subtraction method removes a large portion of the tails of the ZL peak but does not remove all of the effects of the ZL peak. In particular, the subtraction method cannot be used to reveal states within the bandgap. For bandgap EEL spectra a deconvolution is necessary and can reveal bandgap states with high sensitivity. As the low loss represents a joint density of states, while the core loss provides the density of final (empty) states, detailed comparison of the two may now finally provide a reliable method for determining the valence band density of states from localized regions.

Acknowledgements

This work was supported in part by Lockheed Martin Energy Research Corp. under DOE contract no. DE-AC05-96OR22464, and by appointments to the ORNL Postdoctoral Research Associates program administered jointly by ORNL and ORISE.

References

1 Rafferty B and Brown L M (1998) Direct and indirect transitions in the region of the bandgap using electron-energy-loss spectroscopy. *Phys. Rev. B* **58**: 10326–10337.

2 Bangert U, Harvey A J, Freundt D, and Keyse R (1997) Highly spatially resolved electron energy-loss spectroscopy in the bandgap region of GaN. *J. Microsc.* **188**: 237–242.

3 Egerton R F (1989) *Electron Energy Loss Spectroscopy in the Electron Microscope* (Plenum Press, New York).

4 Batson P E, Johnson D W, and Spence J C H (1992) Resolution enhancement by deconvolution using a field emission source in electron energy loss spectroscopy. *Ultramicroscopy* **41**: 137–145.

5 Issacson M and Scheinfein M (1983) A high performance electron energy loss spectrometer for use with a dedicated STEM. *J. Vac. Sci. Technol. B* **1**: 1338–1343.

6 Rafferty B (1997) Thesis, Cambridge University.

7 Fowler R H and Nordheim L (1928) Electron emission in intense electric fields. *Proc. Roy. Soc. London A* **119**: 173–181.

8 Gadzuk J W and Plummer E W (1973) Field emission energy distribution (FEED). *Rev. Mod. Phys.* **45**: 487–548.

9 Garcia-Molina R, Gras-Marti A, and Ritchie R H (1985) Excitation of edge modes in the interaction of electron beams with dielectric wedges. *Phys. Rev. B* **31**: 121–126.

10 Garcia-Molina R, Gras-Marti A, Howie A, and Ritchie R H (1985) Retardation effects in the interaction of charged particle beams with bound condensed media. *J. Phys. C: Solid State Phys.* **18**: 5335–5345.

11 Echinique P M, Flores F, and Ritchie R H (1991) Image potential effects of low and high energy electrons. *Surf. Sci.* **251/252**: 119–126.

12 Barrera R G and Fuchs R (1995) Theory of electron energy loss in a random system of spheres. *Phys. Rev. B* **52**: 3256–3273.

13 Aizpuria J and Rafferty B (1997) Numerical simulation of valence losses in MgO cubes. *Inst. Phys. Conf. Ser.* **153**: 277–280.

14 Walls M G (1987) Thesis, Cambridge University.

15 Henrich V E (1980) Energy-dependent electron energy loss spectroscopy: application to the surface and bulk electronic structure of MgO. *Phys. Rev. B* **22**: 4764–4775.

16 Kassim H A, Matthew J A D, and Green B (1977) Electronic structure of the surface F centre in ionic crystals. *Surf. Sci.* **74**: 109–124.

17 Batson P E (1999) Advanced spatially resolved EELS in the STEM. *Ultramicroscopy* **78**: 33–42.